



HAL
open science

Reduced nonradiative recombination in semipolar green-emitting III-N quantum wells with strain-reducing AlInN buffer layers

Philipp Henning, Philipp Horenburg, Heiko Bremers, Uwe Rossow, Florian Tendille, Philippe Vennégués, Philippe de Mierry, Jesus Zúñiga-Pérez, Andreas Hangleiter

► To cite this version:

Philipp Henning, Philipp Horenburg, Heiko Bremers, Uwe Rossow, Florian Tendille, et al.. Reduced nonradiative recombination in semipolar green-emitting III-N quantum wells with strain-reducing AlInN buffer layers. *Applied Physics Letters*, 2019, 115 (20), pp.202103. 10.1063/1.5118853. hal-03023684

HAL Id: hal-03023684

<https://hal.science/hal-03023684v1>

Submitted on 25 Nov 2020

HAL is a multi-disciplinary open access archive for the deposit and dissemination of scientific research documents, whether they are published or not. The documents may come from teaching and research institutions in France or abroad, or from public or private research centers.

L'archive ouverte pluridisciplinaire **HAL**, est destinée au dépôt et à la diffusion de documents scientifiques de niveau recherche, publiés ou non, émanant des établissements d'enseignement et de recherche français ou étrangers, des laboratoires publics ou privés.

Reduced nonradiative recombination in semipolar green-emitting III-N quantum wells with strain-reducing AlInN buffer layers

Cite as: Appl. Phys. Lett. **115**, 202103 (2019); <https://doi.org/10.1063/1.5118853>

Submitted: 05 July 2019 . Accepted: 02 November 2019 . Published Online: 14 November 2019

Philipp Henning , Philipp Horenburg, Heiko Bremers, Uwe Rossow, Florian Tendille, Philippe Vennégués , Philippe de Mierry, Jesús Zúñiga-Pérez , and Andreas Hangleiter 



View Online



Export Citation



CrossMark

ARTICLES YOU MAY BE INTERESTED IN

[Evidence of trap-assisted Auger recombination in low radiative efficiency MBE-grown III-nitride LEDs](#)

Journal of Applied Physics **126**, 184502 (2019); <https://doi.org/10.1063/1.5096773>

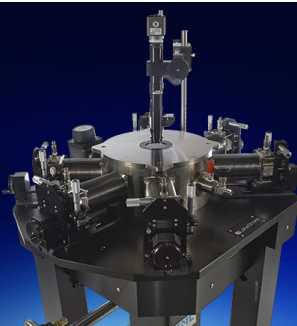
[Multi-wave mixing using a single vector optical field](#)

Applied Physics Letters **115**, 201104 (2019); <https://doi.org/10.1063/1.5121785>

[Unusual electric field-induced optical behaviors in cesium lead bromide perovskites](#)

Applied Physics Letters **115**, 201101 (2019); <https://doi.org/10.1063/1.5116326>

 **Lake Shore**
CRYOTRONICS



Cryogenic probe stations

for accurate, repeatable
material measurements

LEARN MORE 

AIP
Publishing

Reduced nonradiative recombination in semipolar green-emitting III-N quantum wells with strain-reducing AlInN buffer layers

Cite as: Appl. Phys. Lett. **115**, 202103 (2019); doi: [10.1063/1.5118853](https://doi.org/10.1063/1.5118853)

Submitted: 5 July 2019 · Accepted: 2 November 2019 ·

Published Online: 13 November 2019






View Online



Export Citation



CrossMark

Philipp Henning,^{1,2,a)}  Philipp Horenburg,^{1,2} Heiko Bremers,^{1,2} Uwe Rossow,^{1,2} Florian Tendille,³ Philippe Vennégués,³  Philippe de Mierry,³ Jesús Zúñiga-Pérez,³  and Andreas Hangleiter^{1,2} 

AFFILIATIONS

¹Institute of Applied Physics, Technische Universität Braunschweig, Mendelssohnstr. 2, 38106 Braunschweig, Germany

²Laboratory for Emerging Nanometrology, Technische Universität Braunschweig, Langer Kamp 6a, 38106 Braunschweig, Germany

³Centre de Recherche sur l'Hétéro-Epitaxie (CNRS-CRHEA), Rue Bernard Grégory, 06560 Valbonne, France

^{a)}Electronic mail: p.henning@tu-bs.de

ABSTRACT

Using strain-reducing partially relaxed AlInN buffer layers, we observe reduced nonradiative recombination in semipolar green-emitting GaInN/GaN quantum wells. Since strain is a key issue for the formation of defects that act as nonradiative recombination centers, we aim to reduce the lattice mismatch between GaInN and GaN by introducing an AlInN buffer layer that can be grown lattice-matched along one of the in-plane directions of GaN, even in the semipolar (11 $\bar{2}2$) orientation. With the increasing thickness, the buffer layer shows partial relaxation in one direction and thereby provides a growth template with reduced lattice mismatch for the subsequent GaInN quantum wells. Time-resolved photoluminescence measurements show reduced nonradiative recombination for the structures with a strain-reducing buffer layer.

Published under license by AIP Publishing. <https://doi.org/10.1063/1.5118853>

With optoelectronic devices based on GaInN quantum wells (QWs), high efficiencies are achieved, particularly in the violet and blue spectral regions. In order to achieve light emission at longer wavelengths, high InN mole fractions are required. Generally, this goes along with a drastic reduction of the device efficiency, which is known as the “green gap.”^{1,2} On the one hand, this phenomenon can be attributed to the internal polarization fields on *c*-plane structures. Since in these structures high internal polarization fields are present, their radiative emission is governed by the quantum-confined Stark effect³ (QCSE) that reduces the radiative oscillator strength.⁴ One possibility to reduce the impact of polarization fields on the device performance is structures in non- and semipolar crystal orientations.^{5,6}

On the other hand, the realization of high indium contents required for green-emitting GaInN QW structures is difficult in terms of strain.^{7–9} Langer *et al.* have found that strain is a key issue to understand the green gap, since the large lattice mismatch between GaN and high-indium containing *c*-plane GaInN QWs leads to the formation of strain-induced defects.¹⁰ In order to reduce the lattice mismatch, buffer layers can be incorporated into the structures prior to the QWs. One possibility is the use of GaInN layers with a low indium content, which has been shown to improve the performance of light-emitting

and laser devices on several semipolar planes.^{11–13} Using GaInN, however, the reduction in lattice mismatch is limited, since the indium composition needs to be low to avoid reabsorption of the QW emission. Another suitable material is AlInN, which is of particular interest since it can be grown lattice-matched to GaN in *c*-plane orientation at an InN mole fraction of approximately 18% according to Vegard's rule.¹⁴ Due to the different *a/c*-ratios of the binary III-N materials, the lattice-matching can be achieved only in one of the in-plane directions for non- and semipolar crystal orientations. Earlier work focused on QWs grown on nonpolar *m*-plane substrates, where the AlInN layers were successfully used for strain management in a multiquantum well (MQW) structure.^{15,16}

In the present work, we address the influence of the growth substrate and a strain-reducing AlInN buffer layer on nonradiative recombination in GaInN/GaN QW structures grown on semipolar (11 $\bar{2}2$) GaN templates to check whether a similar defect formation mechanism as found by Langer *et al.*¹⁰ on the *c*-plane can be observed. On (11 $\bar{2}2$) GaN, AlInN can be grown lattice-matched to the [11 $\bar{2}3$] (or *c'*-direction) at a 25.8% InN mole fraction and is compressively strained ($\approx -1.04\%$) in the other in-plane direction, [1 $\bar{1}00$] or *m*-direction. Earlier work focused on relaxation of AlInN layers of

varying thicknesses and found that by choosing lattice-matching along the c' -direction, the AlInN layer is forced to relax to larger m lattice parameters, which effectively reduces the lattice mismatch to the subsequent MQW structure based on GaInN.^{15,17} Lattice-matching along m would leave AlInN under tensile strain in c' ($\approx +1.03\%$), and relaxation would lead to smaller c' lattice parameters and an even larger lattice mismatch between the relaxed AlInN and GaInN QWs. Time-resolved photoluminescence measurements presented in this work show a reduced nonradiative recombination for the structures with a partially relaxed AlInN buffer layer.

For the analysis, five samples in (1122) orientation are prepared by low pressure metalorganic vapor phase epitaxy (MOVPE) in a commercial Aixtron AIX200RF reactor. The structural characterization is carried out by high-resolution x-ray diffraction (XRD).^{18,19} The samples are grown on pseudobulk GaN (sample A) or GaN templates (samples B1, B2, C1, and C2) on patterned and overgrown r -plane sapphire, see Fig. 1(a). The details on the template preparation were reported elsewhere.^{20,21} The growth starts with epitaxial GaN, followed by a low-temperature GaN underlayer of about 20 nm thickness.²² The growth of the fivefold GaInN/GaN multiquantum well (MQW) structure is following, with QW growth temperatures of 740 °C (samples A, B1, and C1), resulting in 35%–37% InN mole fraction, or 770 °C (samples B2 and C2), resulting in 27%–29% InN mole fraction. Comparable barrier widths of approximately 8 nm and QW widths between 1.2 and 1.56 nm are found for all samples. An additional AlInN buffer layer is inserted underneath the MQW in samples A, B1, and B2. It is grown for 100–200 min at 820 °C, resulting in layer thicknesses of 250–500 nm and an InN mole fraction around 26%, as confirmed by XRD. Moreover, no evidence of phase separation in AlInN is found. The summarized results of the structural analysis can be found in Table I and Fig. 1.

Figure 1(b) shows reciprocal space maps (RSMs) of the 0222 and 0006 reflections. Besides the GaN substrate peaks, also the AlInN peaks and the MQW superlattice (SL) peaks are visible. The reflections of GaN and AlInN are aligned in the in-plane direction (Q_{\parallel}) in both RSMs (0222 and 0006), which proves coherently strained growth of AlInN on the GaN template. In the 0222 RSM, an asymmetrical AlInN peak indicates relaxation in the m -direction toward larger lattice parameters. The MQW SL peaks are aligned with the relaxed part of the AlInN peak, indicating pseudomorphic growth of the QWs on the partially relaxed buffer layer. In the 0006 RSM, no asymmetry can be found in the AlInN peak, which proves that lattice matching is

conserved in the c' -direction. The RSMs of samples C1/C2 (not shown) prove pseudomorphic growth of the MQW on the GaN template without an AlInN buffer layer. Since the XRD scans average over a large sample volume, no direct information about the relaxation of AlInN at the interface to the MQW region can be obtained. Thus, the (1100) in-plane lattice parameters are evaluated by 2θ scans in grazing incidence geometry, as shown in Fig. 1(c) for samples A, B1, and C1. Since the scan is sensitive only to some tens of nanometers at the top of the structure, the values correspond to the lattice parameters of the upper layers in the MQW structure. For sample C1, the in-plane lattice parameter of free-standing GaN is found, indicating pseudomorphic growth of the QWs on the GaN template. The change to larger lattice parameters for samples A and B1 can be directly linked to the partially relaxed AlInN buffer layer, which shows $(15 \pm 5)\%$ (sample A) and $(51 \pm 5)\%$ (sample B1) relaxation in the m -direction, assuming that the in-plane lattice parameters of AlInN and MQW are equal. Furthermore, for sample C2 (not shown), the same in-plane lattice parameter as for sample C1 is obtained, while for the AlInN layer in sample B2 (not shown), $(49 \pm 5)\%$ relaxation is found, close to sample B1. Further details on the structural characterization of the AlInN layers can be found in the supplementary material and in Refs. 15 and 17 where the relaxation of AlInN layers grown under identical conditions are examined. There, the same trend in relaxation is found, although the absolute degree of relaxation seems to be higher. In summary, the structural characterization shows that the AlInN buffer layer reduces the lattice mismatch for the GaInN QWs as intended.

For the time-resolved photoluminescence measurements, the second harmonic of a 35 fs-Ti:sapphire laser is used to excite the QWs resonantly with laser pulses of 410 nm wavelength in a confocal setup with focal sizes of several micrometers. The excitation energy density is below $100 \mu\text{J cm}^{-2}$. The samples are mounted in a continuous flow cryostat to vary the temperature between 5 and 300 K. The collected PL light is dispersed by a 30 cm spectrograph with 150/mm grating and finally detected by a streak camera (Hamamatsu C10910) with a temporal resolution better than 10 ps. The photoluminescence decays are measured with a repetition rate of 80 MHz and spectrally integrated to include a window where the intensity exceeds 10% of the peak value. A convolution of a monoexponential decay [$\propto I_0 \exp(-t/\tau_{\text{eff}})$] and a Gaussian function is used to fit the obtained transients.²³ From the fit, the initial intensity I_0 and the effective lifetime τ_{eff} are determined that can be split into a radiative (τ_r) and a nonradiative lifetime (τ_{nr}) using the relation

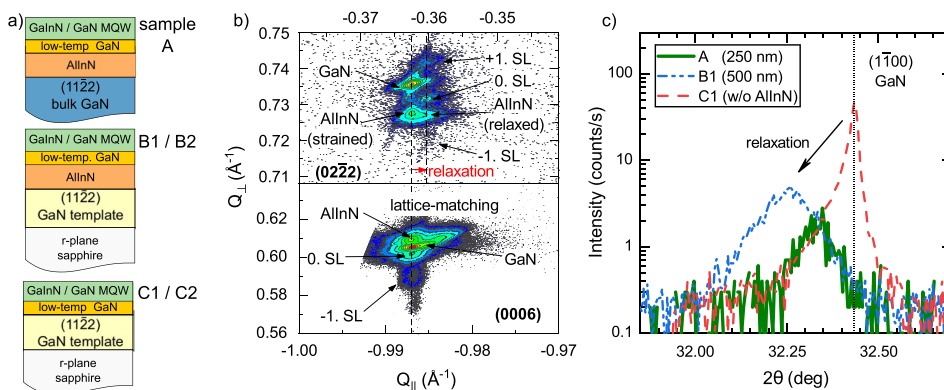


FIG. 1. Schematic of the sample structure (a) and reciprocal space maps (b) of the (0222) reflex showing strained AlInN growth and subsequent relaxation along m , and the (0006) reflex showing lattice matching in the c' -direction. XRD 2θ scans in grazing-incidence geometry of the in-plane (1100) reflex (d) show the lattice parameter of free-standing GaN for sample C1 (proving pseudomorphic growth on the template without the buffer layer) and increasing relaxation to larger in-plane lattice parameters for samples A and B1 with an additional AlInN buffer layer.

TABLE I. Basic information on the investigated samples, listing the growth duration of the AlInN buffer layer (d_{buffer}), its approximate thickness (t_{buffer}) and degree of relaxation in the m -direction ($R_{m,\text{buffer}}$), the InN mole fraction of AlInN (y_{buffer}) and the MQW (x_{QW}), the QW width (t_{QW}), the emission wavelength at 300 K ($\lambda_{300\text{K}}$), and the effective lifetimes at 5 K ($\tau_{5\text{K}}$) and 300 K ($\tau_{300\text{K}}$), as well as the radiative lifetimes at 300 K ($\tau_{r,300\text{K}}$). The barrier width is approximately 8 nm for all the samples.

Sample	d_{buffer} (min)	t_{buffer} (nm)	$R_{m,\text{buffer}}$ (%)	y_{buffer} (%)	t_{QW} (nm)	x_{QW} (%)	$\lambda_{300\text{K}}$ (nm)	$\tau_{5\text{K}}$ (ps)	$\tau_{300\text{K}}$ (ps)	$\tau_{r,300\text{K}}$ (ps)
A	100	≈ 250	15 ± 5	26.5 ± 0.3	1.48 ± 0.05	36 ± 1	543	191 ± 2	66 ± 3	1720 ± 500
B1	200	≈ 500	51 ± 5	25.7 ± 0.4	1.46 ± 0.06	37 ± 1	576	168 ± 4	74 ± 2	1600 ± 250
B2	200	≈ 500	49 ± 5	26.9 ± 0.6	1.4 ± 0.1	27 ± 1	497	133 ± 2	81 ± 2	410 ± 70
C1	1.56 ± 0.06	36 ± 1	536	108 ± 2	34 ± 2	2240 ± 450
C2	1.2 ± 0.1	29 ± 1	492	61 ± 2	45 ± 2	313 ± 65

$$\frac{1}{\tau_{\text{eff}}} = \frac{1}{\tau_r} + \frac{1}{\tau_{\text{nr}}} \quad (1)$$

Due to the short-pulse excitation, the radiative rate is proportional to the initial intensity I_0 . Thus, the radiative lifetimes $\tau_r \propto 1/I_0$ can be determined by applying a low temperature normalization, where the effective lifetime τ_{eff} is assumed to equal the radiative lifetime τ_r at 5 K.¹⁰ Figure 2(a) shows PL spectra of all samples, where full widths at half maximum of 150–200 meV can be observed. Furthermore, scanning the sample surface with a focal size of approximately $2 \mu\text{m}$ shows that the effective PL decay times remain constant.

An exemplary measurement of the temperature-dependent lifetimes is shown in Fig. 2(b) for sample B1. While the recombination is assumed to be purely radiative at low temperatures, the lifetimes are clearly dominated by nonradiative recombination at room temperature (300 K). At low temperatures, the recombining charge carriers may be subject to localization at potential minima, originating from fluctuations of the QW composition or width.^{24–28} Since the radiative lifetime scales with temperature according to the dimensionality d of the recombining charge carriers ($\tau_r \propto T^{d/2}$),²⁹ the constant radiative lifetimes at low temperature in fact indicate the localization of charge carriers. As the radiative lifetimes show a close to linear increase toward elevated temperatures, the charge carriers have to be considered free in two dimensions after thermal escape from the potential minima. The measured lifetimes of the other samples show a comparable behavior, and the absolute values for the lifetimes at 5 and 300 K can be found in Table I. At 300 K, we see no significant difference in radiative lifetimes for samples with the same InN mole fraction. Thus, possible strain-induced changes of the valence band structure do not affect the radiative recombination.

In order to compare the impact of an AlInN buffer layer on the recombination properties, the effective lifetimes at 300 K are considered, where the nonradiative recombination is dominant for all samples. Still, the measurements show significantly different lifetimes. Although the recombination at low temperatures is assumed purely radiative, there is the possibility of remaining nonradiative recombination, which would affect the low temperature normalization used to split the measured lifetimes into radiative and nonradiative lifetimes. Specifically, for sample C2, which shows a lower lifetime at 5 K compared to the other samples, it cannot be ruled out that the decay is at least partially nonradiative at low temperatures. Even if this is the case for one or more of the samples, the measured effective lifetimes at 300 K remain unchanged and are a suitable measure for the nonradiative recombination.

For better comparison, the normalized room temperature transients are displayed in Fig. 2(c). It can be clearly seen that the samples without a buffer layer (C1 and C2) show faster nonradiative decays than the ones with an additional AlInN buffer layer (A, B1, and B2), which is confirmed by the fitted lifetimes. All the samples with an AlInN buffer layer show effective lifetimes between 66 ps (A) and 81 ps (B2), which are significantly higher than 34 ps (C1) and 45 ps (C2) of the unbuffered samples. Since the measured lifetimes provide an absolute measure for the nonradiative recombination rate, this result proves a reduced nonradiative recombination for structures with an AlInN buffer layer. Comparing the room temperature lifetimes of samples with the same QW composition, the nonradiative rate is reduced by a factor of approximately 2. Furthermore, the degree of relaxation of the AlInN buffer has an effect on the nonradiative recombination, since sample A (15% relaxation) shows a shorter lifetime of 66 ps compared to samples B1 and B2 ($\approx 50\%$ relaxation) with 74 ps and 81 ps.

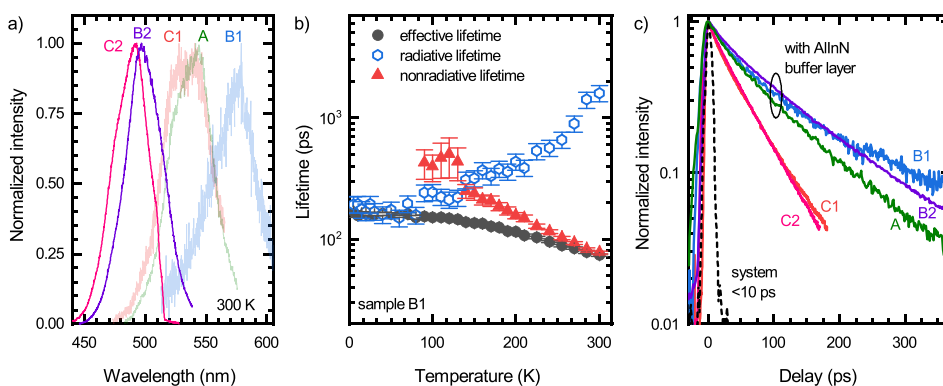


FIG. 2. Spectra at 300 K (a), temperature-dependence of the effective, radiative, and nonradiative lifetimes for sample B1 (b), where the nonradiative recombination is dominant at 300 K, and transients at 300 K (c), where the samples without a buffer layer (C1 and C2) show a faster decay than the samples with a partially relaxed buffer layer (A, B1, and B2), indicating a significant reduction of the nonradiative recombination.

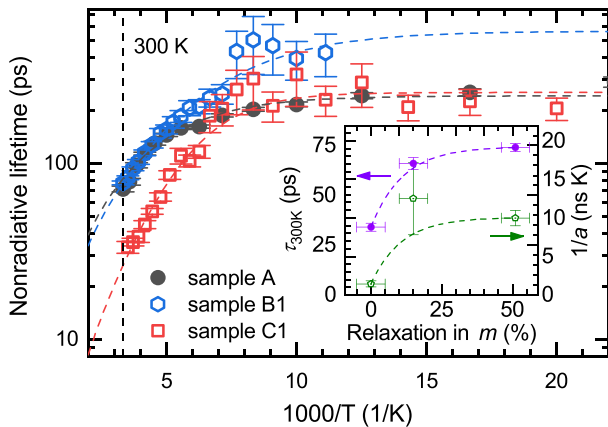


FIG. 3. Arrhenius-type graph of the nonradiative lifetimes of samples A, B1, and C1, where a similar slope indicates comparable activation energies. Dashed lines represent fits according to Eq. (2). The inset shows the inverse of prefactor $1/a$, related to the density of nonradiative centers, and the room temperature lifetimes as a function of relaxation in m -direction. Dashed lines in the inset serve as guides to the eye.

and 81 ps, respectively. To investigate the origin of the reduced nonradiative recombination, an Arrhenius-type plot of the nonradiative lifetimes is given in Fig. 3 for samples A, B1, and C1. The thermal activation of the nonradiative recombination can be described by

$$\frac{1}{\tau_{\text{nr}}} = a(T) \exp\left(-\frac{E_{\text{act}}}{k_{\text{B}}T}\right) + \frac{1}{\tau_0}, \quad (2)$$

where k_{B} is Boltzmann's constant and E_{act} is a characteristic activation energy for the nonradiative process. The prefactor $a(T)$, scaling with the density of nonradiative centers, is assumed to depend linearly on temperature, according to the effective density of states. The actual temperature dependence may, however, change depending on the charge state of the nonradiative center.³⁰ The temperature-independent contribution $1/\tau_0$ accounts for possible remaining nonradiative recombination at low temperatures due to tunneling of charge carriers to nonradiative centers.³¹ As can be seen from Table II, samples A and B1 show similar activation energies below 30 meV, indicating that the same nonradiative recombination mechanism is dominant in both structures. In contrast, sample C1 without a buffer layer shows a larger activation energy of 46 meV. This might indicate a change in the nonradiative mechanism compared to the buffered samples but is still in the same order of magnitude as 30 meV of samples

TABLE II. Results of the Arrhenius-type fits according to Eq. (2) for samples A, B1, and C1, listing the prefactor a related to the density of nonradiative centers, i.e., defects in the QW, the characteristic activation energy E_{act} for the nonradiative recombination process, and the parameter $1/\tau_0$ related to remaining nonradiative recombination at low temperatures.

Sample	a ($\text{ns}^{-1} \text{K}^{-1}$)	E_{act} (meV)	$\frac{1}{\tau_0}$ (ns^{-1})
A	0.08 ± 0.03	29 ± 7	4.1 ± 0.3
B1	0.10 ± 0.01	25 ± 4	1.7 ± 0.4
C1	0.7 ± 0.2	46 ± 5	4.0 ± 0.4

A and B1. Also, the prefactor a for sample C1 is significantly higher than for sample B1, indicating a higher defect density in the QWs without buffer layer, while no significant difference between samples B1 and A can be observed. This is shown in Fig. 3, where the effective lifetimes increase with increasing relaxation of the AlInN layer, and also the prefactors related to the defect density follow this behavior when the inverse $1/a$ is plotted for comparable dimensions. Within the uncertainties, the reduced nonradiative recombination and the lower defect densities in the QWs with increasing relaxation of the AlInN buffer layer follow the same trend.

Considering the parameter $1/\tau_0$, tunneling to nonradiative centers cannot be excluded at low temperatures, in particular, for samples A and C1. Moreover, the formation of additional defects in the AlInN layer during relaxation is possible. Although the formation of in-plane misfit dislocations is most likely,^{17,32} threading dislocations with an out-of-plane component could be formed in AlInN. Those defects could penetrate into the QWs and give rise to additional nonradiative recombination. Since the overall nonradiative rate is decreased with an AlInN layer, the overall defect density is decreased rather than increased. Furthermore, the recombination dynamics do not imply that the structure on the bulk substrate performs better than the ones on patterned sapphire templates. Instead, the recombination dynamics are rather dominated by the reduced strain due to the AlInN layer.

This indicates that nonradiative centers or defects are not related to the dislocations stemming from the template but are generated during growth of the QW region that is subject to high strain. Thus, the overall trend of increasing relaxation of the AlInN buffer and decreasing defect densities in the QWs is consistent with strain-induced formation of defects that act as nonradiative centers. This was suggested by Langer *et al.* for c -plane structures, where the formation of strain-induced defects in the QW was found to be the dominant source of nonradiative recombination.¹⁰ There, pointlike defects or in-plane dislocations formed by local relaxation in the QWs were proposed to explain the exponential dependence of the nonradiative lifetimes on strain energy density. Although the microscopic origin of the nonradiative centers cannot be evaluated from optical data, a similar mechanism might apply to semipolar orientations as well.

One might suspect that indium in AlInN itself is involved in the process of reducing defects in the QWs, as recently reported by Haller *et al.*^{33–35} for c -plane QWs, where a reduction in the nonradiative recombination is observed when an indium-containing underlayer grown at low temperatures is inserted before the QW structure. As mentioned in the beginning, all the samples investigated here include a similar low-temperature GaN underlayer of about 20 nm thickness. QW structures with such an indium-free underlayer grown on the c -plane achieve 80%–90% internal quantum efficiency (IQE) at room temperature.³⁶ Furthermore, Haller *et al.* observe no additional reduction of the nonradiative recombination for AlInN layer thicknesses above 50 nm.^{34,35} In contrast, in the present work, a reduction of the nonradiative recombination is observed when the AlInN layer thickness is changed by several hundreds of nanometers, which goes along with a significant reduction of the strain in the QW structure. Although a possible effect of indium in the buffer layer on the nonradiative recombination cannot be excluded, it does not seem to be dominating in the present study.

In summary, the use of partially relaxed AlInN buffer layers is found to reduce the nonradiative recombination in semipolar green-emitting GaInN/GaN QWs. The buffer layer is lattice-matched to one of the in-plane directions of GaN and partially relaxed to provide a template with reduced lattice mismatch for the growth of the subsequent QWs. Along with reduced strain in the QWs, a reduced nonradiative recombination rate is observed, on both bulk and overgrown patterned sapphire substrates. Nevertheless, additional optimization of the AlInN buffer layer might help to reduce the nonradiative recombination further.

See the [supplementary material](#) for further details on the XRD analysis of the partially relaxed AlInN buffer layers.

We wish to acknowledge the experimental work performed by Daniel Schmid at the early stage of our investigations.

REFERENCES

- ¹S. Nakamura, M. Senoh, N. Iwasa, and S. Nagahama, *Jpn. J. Appl. Phys., Part 2* **34**, L797 (1995).
- ²T. Mukai, M. Yamada, and S. Nakamura, *Jpn. J. Appl. Phys., Part 1* **38**, 3976 (1999).
- ³T. Takeuchi, S. Sota, M. Katsuragawa, M. Komori, H. Takeuchi, H. Amano, and I. Akasaki, *Jpn. J. Appl. Phys., Part 2* **36**, L382 (1997).
- ⁴J. S. Im, H. Kollmer, J. Off, A. Sohmer, F. Scholz, and A. Hangleiter, *Phys. Rev. B* **57**, R9435 (1998).
- ⁵P. Waltereit, O. Brandt, A. Trampert, H. T. Grahn, J. Menniger, M. Ramsteiner, M. Reiche, and K. H. Ploog, *Nature* **406**, 865 (2000).
- ⁶M. Funato, M. Ueda, Y. Kawakami, Y. Narukawa, T. Kosugi, M. Takahashi, and T. Mukai, *Jpn. J. Appl. Phys., Part 2* **45**, L659 (2006).
- ⁷A. Wakahara, T. Tokuda, X.-Z. Dang, S. Noda, and A. Sasaki, *Appl. Phys. Lett.* **71**, 906 (1997).
- ⁸H. K. Cho, J. Y. Lee, C. S. Kim, G. M. Yang, N. Sharma, and C. Humphreys, *J. Cryst. Growth* **231**, 466 (2001).
- ⁹F. C.-P. Massabuau, S.-L. Sahonta, L. Trinh-Xuan, S. Rhode, T. J. Puchtler, M. J. Kappers, C. J. Humphreys, and R. A. Oliver, *Appl. Phys. Lett.* **101**, 212107 (2012).
- ¹⁰T. Langer, H. Jönen, A. Kruse, H. Bremers, U. Rossow, and A. Hangleiter, *Appl. Phys. Lett.* **103**, 022108 (2013).
- ¹¹P. S. Hsu, M. T. Hardy, F. Wu, I. Koslow, E. C. Young, A. E. Romanov, K. Fujito, D. F. Feezell, S. P. DenBaars, J. S. Speck, and S. Nakamura, *Appl. Phys. Lett.* **100**, 021104 (2012).
- ¹²I. L. Koslow, M. T. Hardy, P. S. Hsu, P.-Y. Dang, F. Wu, A. Romanov, Y.-R. Wu, E. C. Young, S. Nakamura, J. S. Speck, and S. P. DenBaars, *Appl. Phys. Lett.* **101**, 121106 (2012).
- ¹³I. L. Koslow, C. McTaggart, F. Wu, S. Nakamura, J. S. Speck, and S. P. DenBaars, *Appl. Phys. Express* **7**, 031003 (2014).
- ¹⁴L. Vegard, *Z. Phys.* **5**, 17 (1921).
- ¹⁵E. R. Buß, P. Horenburg, U. Rossow, H. Bremers, T. Meisch, M. Caliebe, F. Scholz, and A. Hangleiter, *Phys. Status Solidi B* **253**, 84 (2016).
- ¹⁶P. Horenburg, E. R. Buß, U. Rossow, H. Bremers, F. A. Ketzler, and A. Hangleiter, *Appl. Phys. Lett.* **108**, 102105 (2016).
- ¹⁷E. R. Buß, U. Rossow, H. Bremers, T. Meisch, M. Caliebe, F. Scholz, and A. Hangleiter, *Appl. Phys. Lett.* **105**, 122109 (2014).
- ¹⁸H. Bremers, A. Schwiigel, L. Hoffmann, H. Jönen, U. Rossow, J. Thalmair, J. Zweck, and A. Hangleiter, *Phys. Status Solidi B* **248**, 616 (2011).
- ¹⁹H. Jönen, H. Bremers, U. Rossow, T. Langer, A. Kruse, L. Hoffmann, J. Thalmair, J. Zweck, S. Schwaiger, F. Scholz, and A. Hangleiter, *Semicond. Sci. Technol.* **27**, 024013 (2012).
- ²⁰F. Tendille, P. D. Mierry, P. Vennéguès, S. Chenot, and M. Teisseire, *J. Cryst. Growth* **404**, 177 (2014).
- ²¹F. Tendille, D. Martin, P. Vennéguès, N. Grandjean, and P. De Mierry, *Appl. Phys. Lett.* **109**, 082101 (2016).
- ²²S. P. Chang, C. H. Wang, C. H. Chiu, J. C. Li, Y. S. Lu, Z. Y. Li, H. C. Yang, H. C. Kuo, T. C. Lu, and S. C. Wang, *Appl. Phys. Lett.* **97**, 251114 (2010).
- ²³K. Kúsová and T. Popelář, *J. Appl. Phys.* **125**, 193103 (2019).
- ²⁴S. Chichibu, T. Azuhata, T. Sota, and S. Nakamura, *Appl. Phys. Lett.* **69**, 4188 (1996).
- ²⁵Y. Narukawa, Y. Kawakami, M. Funato, S. Fujita, S. Fujita, and S. Nakamura, *Appl. Phys. Lett.* **70**, 981 (1997).
- ²⁶S. F. Chichibu, A. C. Abare, M. S. Minsky, S. Keller, S. B. Fleischer, J. E. Bowers, E. Hu, U. K. Mishra, L. A. Coldren, S. P. DenBaars, and T. Sota, *Appl. Phys. Lett.* **73**, 2006 (1998).
- ²⁷K. P. O'Donnell, R. W. Martin, and P. G. Middleton, *Phys. Rev. Lett.* **82**, 237 (1999).
- ²⁸Y. Kawakami, Y. Narukawa, K. Omae, S. Fujita, and S. Nakamura, *Phys. Status Solidi A* **178**, 331–336 (2000).
- ²⁹P. T. Landsberg, *Recombination in Semiconductors* (Cambridge University Press, Cambridge, 1991).
- ³⁰R. Pässler, *Phys. Status Solidi B* **85**, 203 (1978).
- ³¹T. Langer, M. Klisch, F. A. Ketzler, H. Jönen, H. Bremers, U. Rossow, T. Meisch, F. Scholz, and A. Hangleiter, *Phys. Status Solidi B* **253**, 133 (2016).
- ³²A. E. Romanov, E. C. Young, F. Wu, A. Tyagi, C. S. Gallinat, S. Nakamura, S. P. DenBaars, and J. S. Speck, *J. Appl. Phys.* **109**, 103522 (2011).
- ³³C. Haller, J.-F. Carlin, G. Jacopin, D. Martin, R. Butté, and N. Grandjean, *Appl. Phys. Lett.* **111**, 262101 (2017).
- ³⁴C. Haller, J.-F. Carlin, G. Jacopin, W. Liu, D. Martin, R. Butté, and N. Grandjean, *Appl. Phys. Lett.* **113**, 111106 (2018).
- ³⁵C. Haller, J.-F. Carlin, M. Mosca, M. D. Rossell, R. Erni, and N. Grandjean, *Appl. Phys. Express* **12**, 034002 (2019).
- ³⁶A. Hangleiter, T. Langer, P. Henning, F. A. Ketzler, H. Bremers, and U. Rossow, *Proc. SPIE* **10532**, 105321P (2018).